40th AIAA/ASME/SAE/ASEE Joint Propulsion Conference & Exhibit
11-14 July 2004, Fort Lauderdale, Florida

AIAA 2004-3955

Fulfillment of the Bohm condition on the 'HPHall' fluid-PIC code

F.I. Parra and E. Ahedo

E.T.S.I. Aeronáuticos, Universidad Politécnica de Madrid, Spain

Abstract

HPHall is a quasineutral code and cannot solve the Debye sheaths at the walls of the discharge chamber. Bohm-type transition conditions, instead of wall conditions, must be implemented at boundaries of the computational domain. It was realized that HPHall does not fulfill these conditions even when fine meshes are used. The cause is found to be on the high sensitivity of the solution to the value of the ion density at the boundary nodes. The HPHall weighting method overestimates that density. Two methods to correct that weighting are proposed and validated.

1 Introduction

Hybrid fluid/particle-in-cell(PIC) codes represent a good trade off between macroscopic-continuous codes and fully kinetic ones for the analysis of Hall thruster discharges. They can deal, within reasonable execution times ($\sim$ hours), with the disparate dynamic scales of electrons and ions, and relatively complex geometries and magnetic field topographies.

The HPHall was developed at the Massachusetts Institute of Technology by M. Fife and M. Martínez-Sánchez [1, 2, 3]. It is a hybrid two-dimensional (2D) code where ions and neutrals are modelled as macro-particles of variable mass and electrons behave as a fluid. Ionization and wall recombination of heavy species are treated with Montecarlo methods. The high anisotropy introduced by the magnetic field, $\boldsymbol{B}$, on the electrons is used to solve separately (by finite elements) the electron motions perpendicular- and parallel- to $\boldsymbol{B}$.

HPHall was completed six years ago and has been proved very useful in the analysis of several thrusters. However, recent theoretical advances on Hall thruster physics and the experience obtained on running the code, have made convenient to revise and improve it. An improvement program was started last year at the Universidad Politécnica de Madrid. The subjects that have been revised or are under revision are the following.

1. Implementation of charge-exchange (CEX) collisions.
2. New accommodation model for wall recombination.
3. Checking of conservation of heavy species magnitudes (mass, energy, etcetera).
4. Comparison with the fully macroscopic model of Ahedo et al. [4].
5. Implementation of the charge-saturated sheath model of Ahedo [5] at the lateral boundaries.
6. Fulfillment of Bohm condition at the lateral domain boundaries.
7. New modelling of wall-collisionality effects on the electron equations.

Points 1 and 2 were commented in internal reports to the program's main sponsor. Point 3 and 4 are being used to validate the code, understand the plasma response, and identify improvements to be done on the fully macroscopic code. Point 5 and initial steps on point 6 were presented in a recent conference [6]. The subject of this paper is point 6. Point 7 will be started next.

A short account of HPHall fundamentals was presented in Ref. [6]. Figure 1 shows the three test meshes and the magnetic field profile to be used in this work. Parameters correspond to a SPT-70 thruster. In order to facilitate the comparison with the macroscopic model of Ref. [4] we are using a rather simple geometry and a B-field satisfying $B_z = 0$ and $B_r \propto 1/r$; in this way $\nabla \cdot \boldsymbol{B} = 0$,

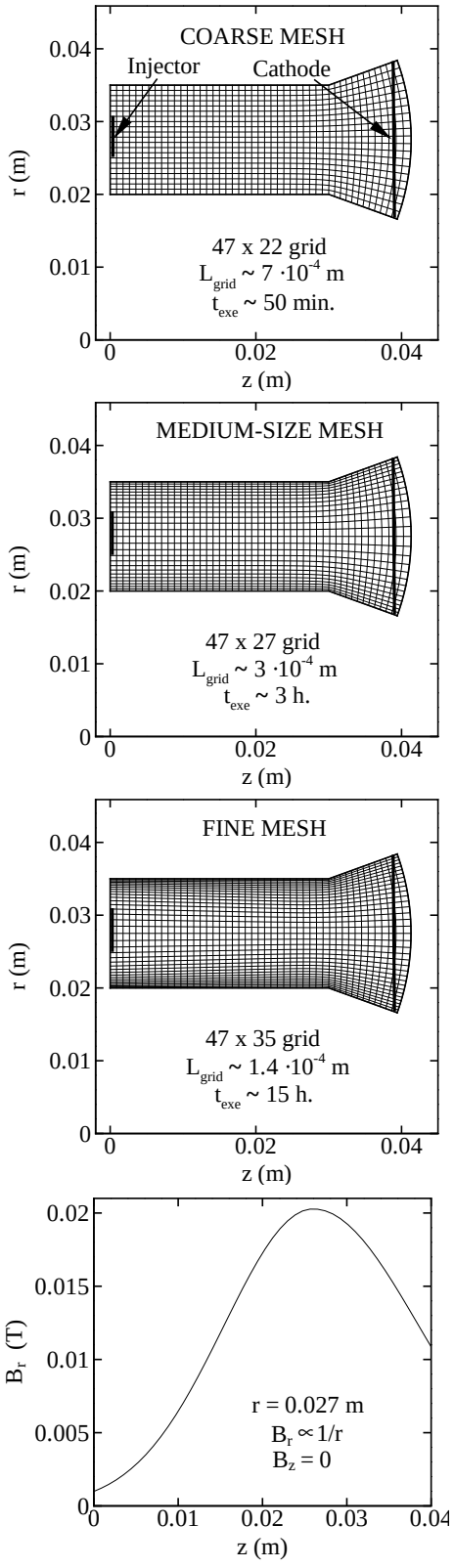

Figure 1: Typical execution times to reach a steady-state response are included.

but $\nabla \wedge \boldsymbol{B} \neq \boldsymbol{0}$. The typical execution times of the coarse(C), medium-size(M) and fine(F) meshes reported in the figure are for a Pentium III at 2.4 GHz.

2 The plasma-wall problem

HPHall is a quasineutral code. Plasma density is computed from a first-order weighting at each mesh node on the surrounding ion macroparticle distribution. The particle density, $n_e = n_i$ (multiple ionization is being disregarded provisionally), and the ion current density, $\boldsymbol{j}_i$, are used as input on the electron equations in order to determine the profiles of the electric potential, ϕ, and the electron temperature, T_e. A good weighting of the plasma density is essential to obtain a reliable plasma response, since ϕ is determined from a Maxwell-Boltzmann law on n_e, and the electric field, which moves the ion particles, is computed from ϕ.

Quasineutrality allows the code to avoid the very short length and time scales associated to the Poisson equation, thus explaining the fast computational time. On the other hand, the main handicap of quasineutrality is that HPHall cannot treat the Debye sheaths surrounding the chamber walls. As a consequence, Debye sheaths must be solved separately and the conditions to be imposed on those boundaries of the computational domain that are next to chamber walls, *are not the wall conditions but the transition conditions to the Debye sheaths.*

SPT thrusters have dielectric walls with high secondary electron emission (SEE). Consistent presheath (quasineutral) and sheath models for this case were developed by Ahedo [5, 7]. The sheath model was implemented in HPHall recently [6]. The solution of the sheath is important mainly to compute electron energy losses, which affect the temperature profile. Here, our interest is on the implementation of the correct condition for the sheath transition, which is known as the Bohm condition.

Figure 2 shows a sketch of the lateral plasma wall interaction, with points W, Q, and T, representing the wall, the sheath transition, and the domain boundary, respectively. Points T and Q should coincide. For the classical case ($T_i \ll T_e$, negligible SEE, and a fluid ion model), the Bohm condition reads

$$v_{riQ} = v_{Bohm} \simeq \sqrt{\frac{kT_e}{m_i}}, \qquad (1)$$

where v_{ri} must be interpreted as the macroscopic velocity component perpendicular to the wall. The

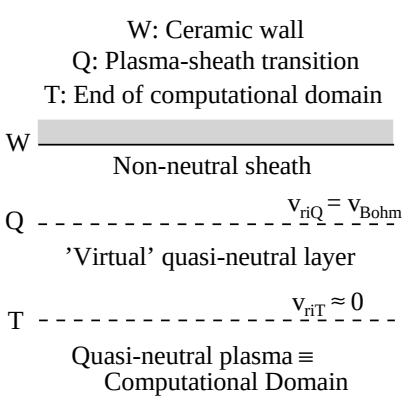

Figure 2: Sketch of the sheath-presheath regions, including the virtual layer assumed implicitly in the original version of the code.

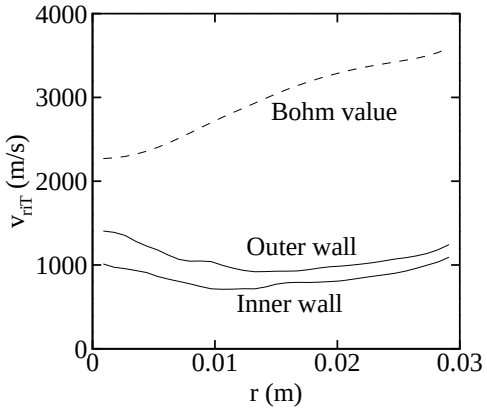

Figure 3: Coarse mesh. Radial ion velocities at the inner and outer boundaries of the computational domain, and the Bohm velocity, $v_{Bohm} \simeq \sqrt{kT_e/m_i}$. Unless otherwise stated, plotted magnitudes in all figures correspond to time-averaged values.

.

thin Debye sheath is collisionless and quasiplanar. Thus, the ion and electron currents are constant along the sheath,

$$j_{r\alpha Q} = j_{r\alpha W}, \quad \alpha = i, e, \tag{2}$$

with $j_{r\alpha} = en_\alpha v_{r\alpha}$. In addition, for a dielectric wall, the two currents must be the same,

$$j_{reW} = j_{riW}, \quad \alpha = i, e. \tag{3}$$

The ion magnitudes at the domain boundary, point T, are obtained from the PIC part of the code. Figure 3 shows that the usual coarse mesh of HPHall yields perpendicular ion velocities (and currents) at the boundaries much smaller than the Bohm value, $v_{riT} \ll v_{Bohm}$. It is well known that plasma velocities and densities present large gradients in the vicinity of the sheath transition. Based on this fact, the original version of HPHall assumed the existence of a quasineutral layer TQ, thinner than the cell radial length but still much thicker than the Debye sheath, where v_{riT} would reach the Bohm value. However, Ref. [6] showed that this layer is inconsistent physically. Therefore, a correct formulation of the HPHall must fulfill necessarily the Bohm condition at the domain boundaries (i.e. T=Q).

The importance of the problem was more evident when the results obtained with the coarse and fine meshes were compared [6]. Figures 4 and 5 illustrate them. [Differences with Figs. 8 to 10 of Ref. [6] are due to improving the re-emission of wall-recombined particles into the chamber.] It was found that:

- The radial plasma structure is much more developed in the fine mesh.
- Differences with the coarse mesh are not limited to a thin region around the boundaries.
- The radial ion current (which is PIC-computed) is typically twice larger with the fine mesh.
- The radial ion velocity is still far from reaching the Bohm value.

The trends of these results suggest that finer meshes would yield larger ion currents and perpendicular ion velocities closer to the Bohm value. However, this does not seem a practical procedure, taking into account the modest advance made from the coarse to the fine mesh, and the cell size and execution time of the fine mesh. Therefore, we decided to investigate directly the way HPHall computes plasma conditions near the boundaries.

3 Fulfillment of the Bohm condition

3.1 Original weighting at boundary nodes

HPHall determines most ion magnitudes (density, velocity, ...) at a mesh node by weighting that magnitude among the particles lying, at each time step, within the volume of influence of that node. For instance, the ion density at a generic node N is determined from

$$(n_{eN})_{weigh} = \frac{1}{\Delta V_N} \sum_p \frac{m_p}{m_i} S_N(r_p, z_p), \tag{4}$$

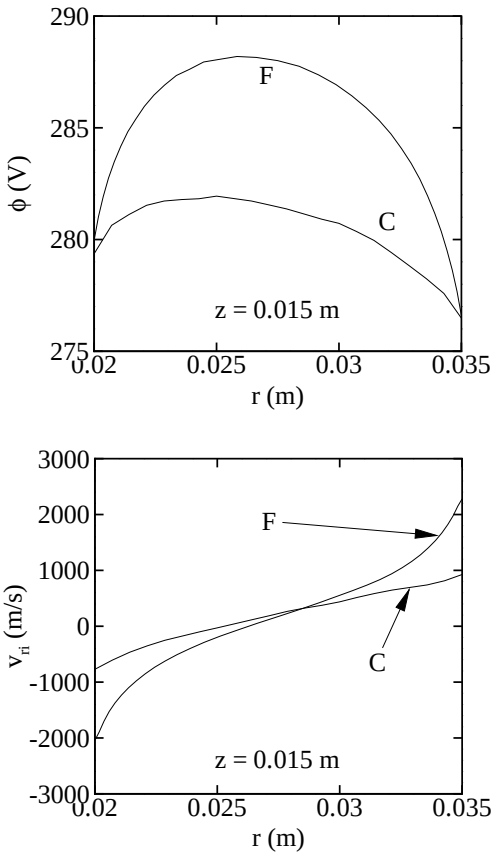

Figure 4: Radial profiles for coarse(C) and fine(F) meshes at $z = 0.015$ m.

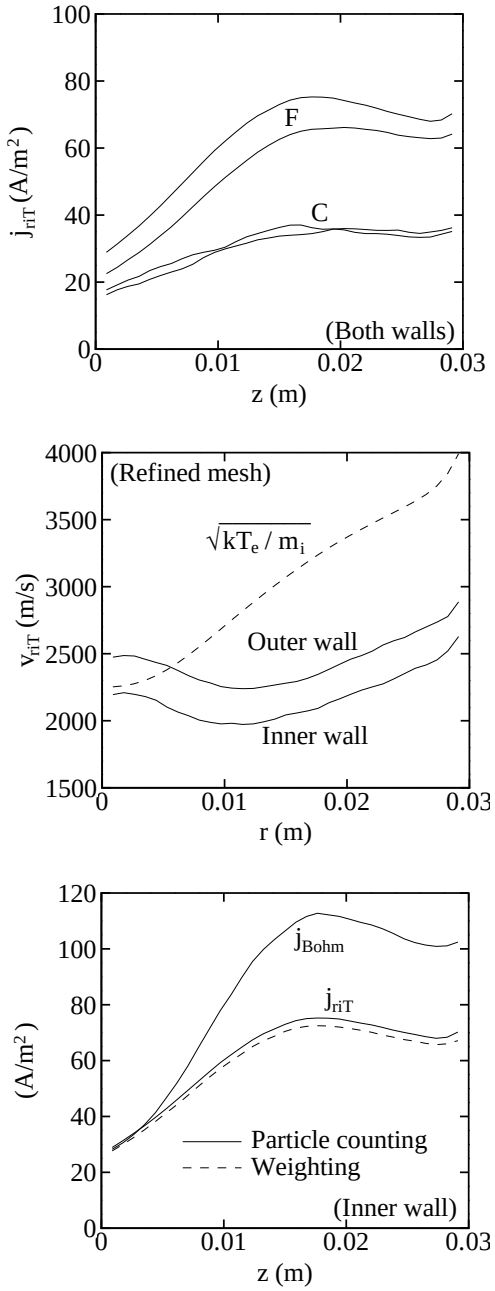

Figure 5: Axial profiles of boundary magnitudes for coarse(C) and fine(F) meshes.

where ΔV_N is the volume associated to node N, p refers to a particle being within the volume of influence of the node, m_p and (r_p, z_p) are particle mass and position, and $S_N(r_p, z_p)$ is a bi-linear type weighting function for node N. Figure 6 sketches the volume of influence of non-boundary and boundary nodes. For the particular case of a rectangular, uniform mesh, with cell sizes Δr and Δz, the volume ΔV_N is 1/4 of the volume of influence, and the weighting function takes the simple form

$$S_N(r_p, z_p) = S_{1N}(r_p) S_{2N}(z_p), \qquad (5)$$

with

$$S_{1N}(r_p) = 1 - \frac{|r_p - r_N|}{\Delta r}$$

and a similar function for $S_{2N}(z_p)$.

Although HPHall weighting favors particles closer to the node, the one-side weighting at the boundary nodes tends to underestimate/overestimate magnitudes that increase/decrease toward the anode. Figure 5 illustrated this point for j_{riT} (a magnitude that increases towards the wall). That current can be computed in two ways: by one-side weighting, $(j_{riT})_{weigh}$, and by counting the particles that cross the boundary,

$$(j_{riT})_{part} = \frac{1}{\Delta t \Delta A_T} \sum_p \frac{e m_p}{m_i}, \qquad (6)$$

with Δt and ΔA_T the simulation time step and the area of the wall panel associated to the node, respectively. Systematically, $(j_{riT})_{part}$, which yields the most correct estimate, is larger than $(j_{riT})_{weigh}$. The error is small for j_{riT} but can be much higher for magnitudes with strong gradients near the sheath transition, like n_{eT} and v_{riT}. Fig. 6(b) illustrates the problem of one-side weighting on n_{eT}.

3.2 Forcing of the Bohm condition

In order to determine whether the no fulfillment of the Bohm condition by HPHall could be due to errors associated to one-side weighting at the lateral boundaries, we decided to modify the computation of the plasma density at a generic boundary node T. The new algorithm would be

$$n_{eT} = \min \left\{ \frac{(j_{riT})_{part}}{e v_{Bohm}}, (n_{eT})_{weigh} \right\} \qquad (7)$$

or, equivalently,

$$v_{riT} = \max \left\{ v_{Bohm}, \frac{(j_{riT})_{part}}{e (n_{eT})_{weigh}} \right\}. \qquad (8)$$

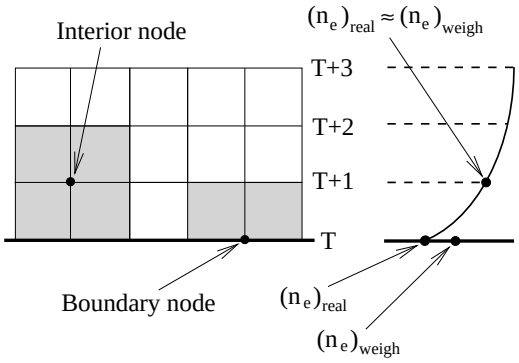

Figure 6: (Left) Shady regions represent the volumes of influence (azimuthal symmetry applies) to weight the heavy-species magnitudes at non-boundary and boundary nodes. (Right) Illustration of errors due to one-side weighting at boundary nodes.

In this way we are forcing the ions to fulfill the Bohm velocity whenever the weighted value of the ion velocity is smaller. With the new definition, n_{eT} is smaller (in most points and instants) than in the original version and, therefore, the electric field is larger near the boundaries.

Figure 7 shows the radial profiles obtained with this method. The local change at the boundary has modified the whole radial profile. The comparison with the original case is really amazing, particularly for the case of the coarse mesh. Applying the Bohm-condition-forcing(BCF), radial profiles are more developed for both meshes. Furthermore, the profiles with BCF are practically identical for the coarse and fine meshes, which gives reliability to this procedure.

Figure 8 shows axial profiles of j_{riT} and v_{riT} at the inner wall (and time-averaged) for the three meshes with BCF. The temperature profiles for the three meshes are practically the same. The fact that $v_{riT} > v_{Bohm}$ is the consequence of temporal fluctuations on the instantaneous value of Eq. (8), and of a non-zero ion temperature. Deviations from the Bohm value are larger for the fine mesh because the instantaneous values of $(v_{riT})_{weigh}$ are larger for that mesh. The differences on the three profiles of j_{riT} and v_{riT} are due to the temporal averaging, mainly.

3.3 Corrected weighting

Bohm condition forcing has demonstrated that correct values of plasma magnitudes at the boundary nodes are essential for a valid solution. At the

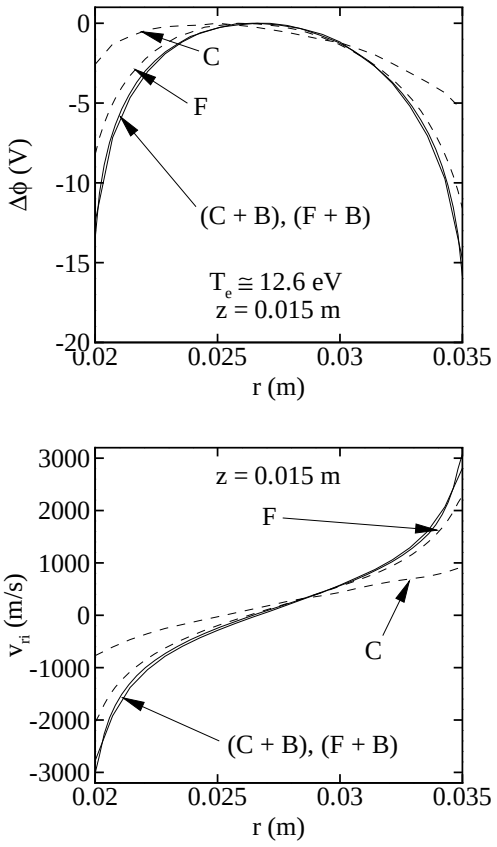

Figure 7: Radial profiles at $z = 0.015$ m for coarse(C) and fine(F) meshes. (+B) means that Bohm condition forcing is applied.

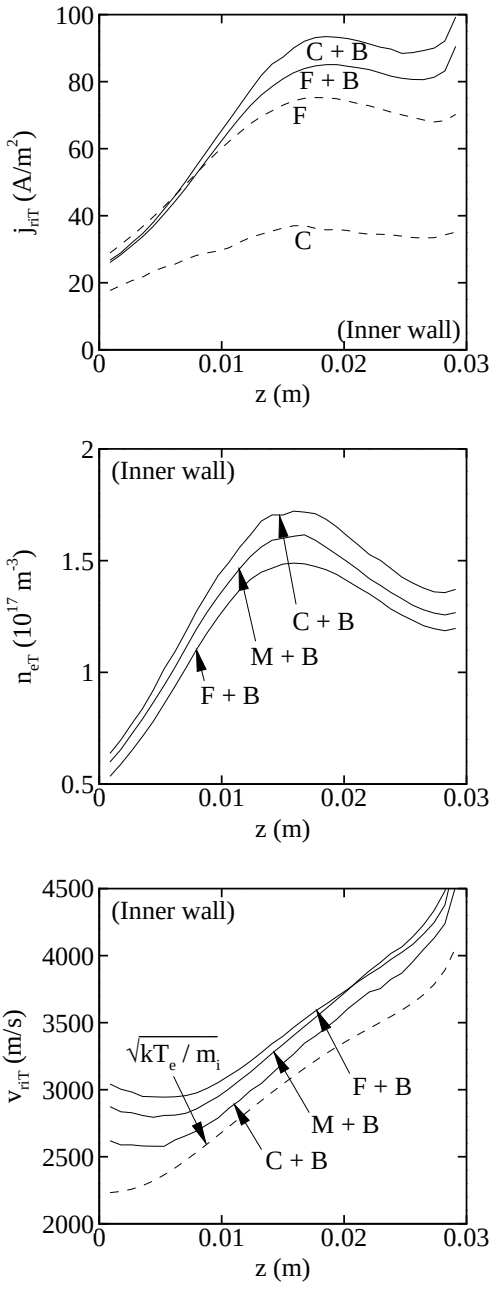

Figure 8: Axial profiles for the three meshes, with(+B) and without Bohm condition forcing.

same time, BCF is an intrusive way to define ion magnitudes, since it relies on a result external to the PIC formulation. Since the domain boundaries of HPHall act as vacuum (ions are lost without any feedback), a well-formulated PIC code should satisfy the Bohm/sonic condition naturally, without forcing it (and, hopefully, without using an infinitely thin mesh).

These considerations leaded us to try to correct the one-side weighting used at the boundary nodes. The idea of our corrected weighting(CW) algorithm is the following. Let us consider that the number of ion macroparticles is high enough, so that the ion density can be represented by a continuous function $n_{e,\,real}(r,z)$. Near the boundary node T, this function can be expanded as

$$n_{e,\,real}(r) = (n_{eT})_{real} + m\ (r - r_T) + O[(r - r_T)^2], \tag{9}$$

where $m = (\partial n_{e,\,real}/\partial r)_T$ (and, for sake of clarity, we omit the dependence on z and, when necessary, we consider a uniform mesh). Equating now the linear weighting of both $n_{e,\,real}(r)$ and the actual PIC macroparticles, yields the following relation:

$$(n_{eT})_{weigh} = \frac{2}{\Delta r}\int_{r_T}^{r_{T+1}} n_{e,\,real}(r) S_{1T}(r) dr = (n_{eT})_{real} + \frac{m}{3}\Delta r + O(\Delta r^2). \tag{10}$$

Applying the same action to the neighbor point T+1 (Fig. 6), one has

$$(n_{e,\,T+1})_{weigh} = (n_{eT})_{real} + m\Delta r + O(\Delta r^2). \tag{11}$$

Solving linear equations (10) and (11), the corrected weighting value of n_{eT} is

$$(n_{eT})_{real} \simeq \frac{3}{2}(n_{eT})_{weigh} - \frac{1}{2}(n_{e,\,T+1})_{weigh} + O(\Delta r^2), \tag{12}$$

which is smaller than $(n_{eT})_{weigh}$ for usual conditions. This correction lies on internal (PIC-computed) magnitudes only, but, at the same time, it depends on a second, neighbor node.

Figure 9 shows radial profiles for the three meshes when CW is used for n_{eT} and v_{riT}. There is a clear improvement with respect to the results with the original weighting. However, the corrected weighting works better the finer is the mesh; in fact, results for the coarse mesh are far from satisfying Bohm condition. This behavior with the mesh size is due to the non-local character of the CW, which presents errors of the order of the square of the cell radial size, $O(\Delta r^2)$.

The comparison of radial profiles when applying BCF and CW to the fine mesh, at the bottom

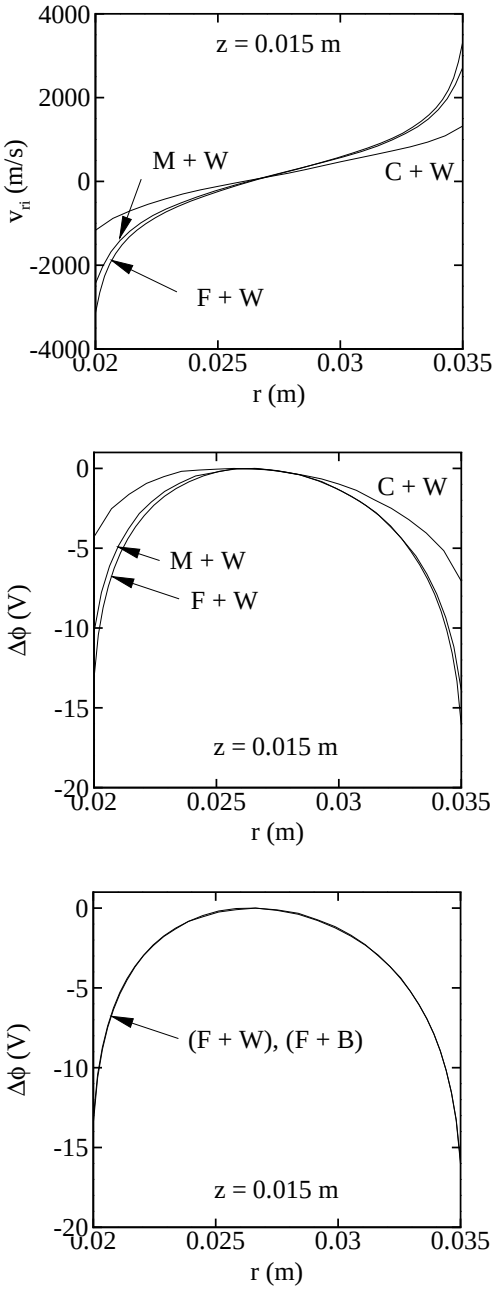

Figure 9: Radial profiles for the three meshes, with(+W) and without application of the corrected weighting algorithm. The bottom figure compares radial profiles when the BCF or the CW are applied together with the fine mesh.

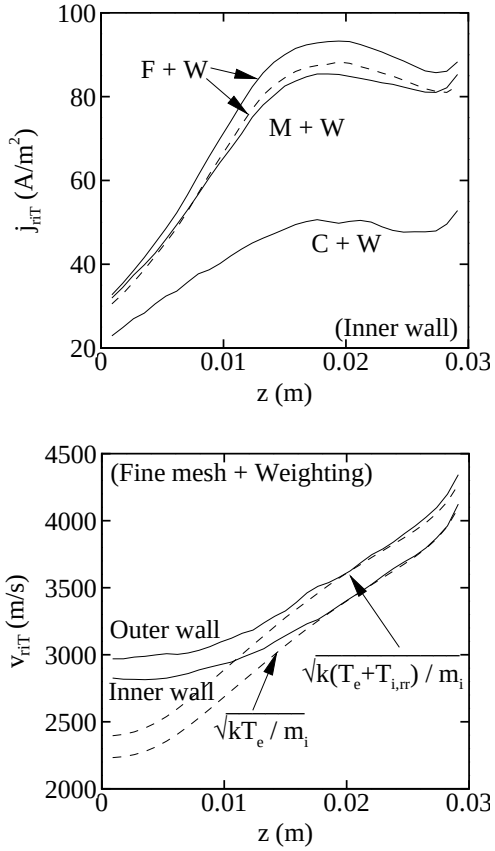

Figure 10: Axial profiles for the three meshes, with (+W) and without application of the corrected weighting algorithm. (Top) Solid lines represent $(j_{riT})_{part}$ and the dashed line shows $e(n_{eT})_{real}(v_{riT})_{real}$ for F+W. (Bottom) $(v_{riT})_{real}$.

of Fig. 9, is excellent, which augments the reliability and accuracy of the methods we are testing. Also, these radial profiles compared very well with those obtained with the radial macroscopic model of Ahedo [7].

Figure 10 depicts axial profiles of boundary magnitudes. It is seen that (for this thruster conditions) the intermediate mesh plus CW yields valid enough results. There are other observations worth to mention. First, there are differences between the radial velocities at the inner and outer walls (in spite of the same electron temperature). These can be due to cylindrical effects on the weighting [8], which are not taken into account in HPHall. Second, the ion velocity at the outer wall seems to include the effect of the ion temperature or, more exactly, of the rr-component of the (weighted) ion pressure tensor, $kT_{i,\,rr} = P_{i,\,rr}/n_i$. Third, v_{riT} tends to exceed clearly the Bohm value in the near anode region. This could be related to larger temporal fluctuations or the low ion fluxes in that region.

4 Final comments

HPHall is a quasineutral code that must satisfy sonic Bohm conditions at the domain boundaries next to chamber walls. The original version of the code was unable to meet this condition even when fine meshes were used. The way of weighting ion magnitudes at the boundary nodes has been identified as the cause of that malfunction of the code.

The problem has been solved with both a one-node, external method (Bohm condition forcing) and a two-node, internal method (corrected weighting algorithm). BCF turns out to be very effective, yielding valid solutions even for coarse meshes. CW works well only for fine enough meshes. For fine meshes both methods yield similar results. These conclusions suggests that BCF should be ordinarily used, whereas CW and fine meshes could be reserved to validate BCF results.

In spite of the very positive results, some improvements on both methods should still be made. First, the general weighting algorithm should take into account cylindrical effects. Second, BCF should try to compensate the effect of temporal fluctuations, which tends to overestimate ion velocities. Third, BCF should include the effect of the ion temperature. Four, a further analysis of the plasma behavior in the near anode region is necessary in order to understand the significant deviations of the radial ion velocity from the Bohm condition.

The ideal solution with respect to the BCF al-

	C MESH		F MESH		
	None	BCF	None	CW	BCF
F(mN)	29	28	30	31	29
P_d(W)	510	489	503	504	475
P_{use}(W)	254	222	244	238	221
η(%)	40	38.9	43	46.1	42.8
η_u(%)	75.2	70.6	72.4	70.9	67.7
P_{ion}(W)	46	55	53	57	53
P_{wall}(W)	176	171	170	173	162

Table 1: HPHall performances for different simulation cases. $V_d = 300$ V, $\dot{m} \simeq 2.1$ mg/s, and $B_{max} \simeq 200$G. This is just an example to compare performances. No attempt to optimize the magnetic field has been made.

gorithm would be to determine the 'internal' Bohm condition from a sheath model based on the actual ion macroparticles that are crossing the sheath.

The Bohm condition must also be satisfied at the anode side of the HPHall domain. BCF and CW algorithms have not been implemented yet at the anode. The implementation is simple for the one-dimensional magnetic field profile considered in this work. On the contrary, for the usual two-dimensional magnetic topography near the anode, the treatment of the whole near-anode region requires a deep revision.

To end, Fig. 11 compares the two-dimensional profiles with and without Bohm condition fulfillment. The larger development of the radial structure of the plasma in the new version of the code is clearly observed. The quasi-symmetry of the profiles with respect to the chamber mid-radius in the new version is another positive feature. However, these important improvements of the code have modest consequences on the computed thruster performances, as Table 1 shows. Two are the reasons: (1) in general, radial gradients are much less significant than axial gradients, (2) the computation of the electron losses at the walls, which dominate the total energy losses, is made by HPHall with an expression independent of the ion flux reaching the walls. The consequences should be larger when wall losses play a lesser role, like for lower discharge voltages, and short and metallic chambers.

Acknowledgments

This research was financed by the European Office for Aerospace Research and Development (Contract Grant FA8655-04-1-3003) and the Ministerio de Ciencia y Tecnología (Project BFM-2001-2352). The firm support of J.M. Fife (Air Force Research Laboratory) and M. Martínez-Sánchez is deeply acknowledged.

References

[1] J.M. Fife and M. Martínez-Sánchez. Two-dimensional hybrid particle-in-cell (PIC) modelling of Hall thrusters. In *24th International Electric Propulsion Conference, Moscow, Russia*, IEPC 95-240. Electric Rocket Propulsion Society, Cleveland, Ohio, 1995.

[2] J.M. Fife, M. Martínez-Sánchez, and J. Szabo. A Numerical Study of Low-Frequency Discharge Oscillations in Hall Thrusters. In *33rd Joint Propulsion Conference, Seattle, WA*, AIAA 97-3052. American Institute of Aeronautics and Astronautics,Washington, DC, 1997.

[3] J. M. Fife. *Hybrid-PIC Modeling and Electrostatic Probe Survey of Hall Thrusters*. PhD thesis, Massachusetts Institute of Technology, 1998.

[4] E. Ahedo, J.M. Gallardo, and M. Martínez-Sánchez. Effects of the radial-plasma wall interaction on the axial Hall thruster discharge. *Physics of Plasmas*, 10(8):3397–3409, 2003.

[5] E. Ahedo. Presheath/sheath model of a plasma with secondary emission from two parallel walls. *Physics of Plasmas*, 9(10):4340–4347, 2002.

[6] F. Parra, E. Ahedo, M. Martínez-Sánchez, and J.M. Fife. Improvement of the plasma-wall model on a fluid-PIC code of a Hall thruster (to be published). In *SP-555: 4th Spacecraft Propulsion Conference, Sardinia (Italy)*, Noordwijk, The Netherlands, 2004. European Space Agency.

[7] E. Ahedo. Radial macroscopic model of a plasma flowing along annular dielectric walls. *Physics of Plasmas*, 9(7):3178–3186, 2002.

[8] J.P. Verboncoeur. Symmetryc spline weighting for charge and current density in particle simulation . *J. Computational Physics*, 174:421 –427, 2001.

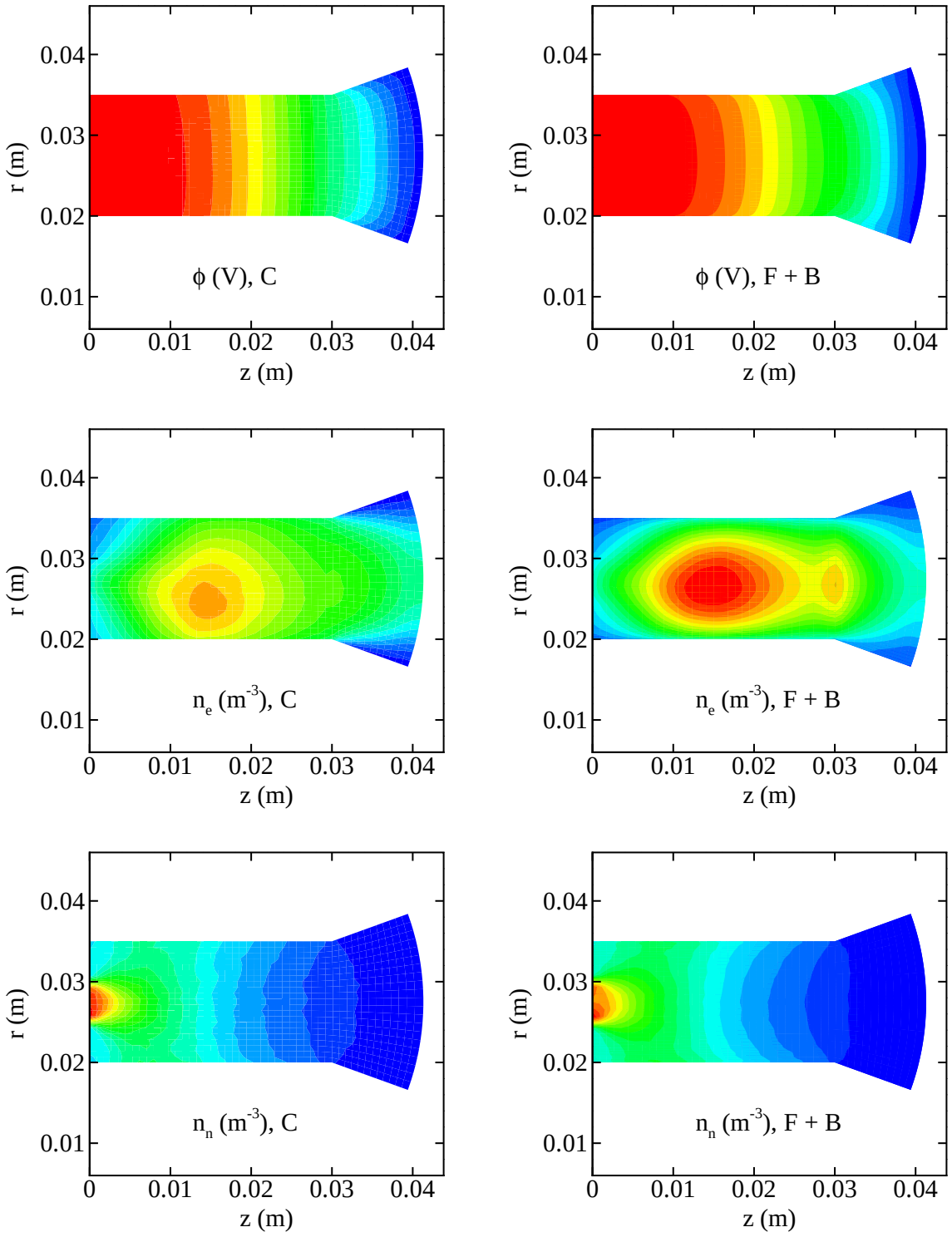

Figure 11: Comparison of two-dimensional contours of the electric potential (top), the plasma density (middle), and the neutral density (bottom), for the coarse mesh (left) and the fine mesh plus Bohm condition forcing (right).